New Materials, Compounds and Applications
Vol.8, No.2, 2024, pp.289-301
https://doi.org/10.62476/nmca82289

INVESTIGATION OF STRUCTURAL, MORPHOLOGY AND OPTICAL PROPERTIES OF GO@METAL OXIDE THIN FILMS PREPARED BY SPRAY PYROLYSIS TECHNIQUE

Mustafa Al-Shuwaili[1,2*], Hdidar Mahdi[1], Megdiche Makram[1]

[1]Composite Material, Ceramics, and Polymers Laboratory, Faculty of Science, Sfax, 3018, Sfax, Tunisia
[2]College of Science, University of Thi-Qar, Nasiriyah, Iraq

Abstract. In this study, spray pyrolysis was used to deposit Graphene Oxide (GO), GO@Ag, GO@Zn, GO@SnO_2, GO@TiO_2, and GO@SiO_2 thin films. Various characterization methods including X-Ray Diffraction (XRD), and Field emission scanning electron microscopy (FESEM), were used to investigate the structural and morphological properties of the prepared thin films. XRD test verify the successfully fabrication of the samples. As seen in the FESEM images, the morphology of the nanocomposites was completely different, which is yet another indication that the nanocomposites were synthesized. In order to study the optical properties of thin films, Photoluminescence (PL) and UV-Visible spectroscopies were used. Among the samples, the one containing TiO_2 nanoparticles showed the best performance in PL and UV-Visible analysis. The reason behind the high photocatalytic activity of GO@TiO_2 nanocomposite is that the titanium ions act as trappings centers, which are beneficial for inhibition of the recombination electron-hole pairs.

Keywords: *graphene oxide, metal oxide, thin film, spray pyrolysis, optical properties, nano composite.*

Corresponding Author: *Mustafa Al-Shuwaili, Composite Material, Ceramics, and Polymers Laboratory, Faculty of Science, Sfax, 3018, Sfax, Tunisia, e-mail: mustafa.khaleel.ph@sci.utq.edu.iq*

Received: *14 June 2024;* ***Accepted:*** *30 July 2024;* ***Published:*** *2 August 2024.*

1. Introduction

Nanostructures comprising different carbon forms, including diamond-like carbon, multiwall carbon nanotubes, single-wall carbon nanotubes, fullerene, and graphene, have garnered significant attention due to their potential in advanced technologies. Graphene, in particular, possesses exceptional properties such as high conductivity, excellent carrier mobility, electromechanical stability, and a large surface area, making it highly promising for applications in photovoltaic devices (Gao *et al*., 2020; Das *et al*., 2020), photodetectors (Shimomura *et al*., 2020; Chen *et al*., 2020), and light-emitting diodes (Moon *et al*., 2020). Graphene consists of a single layer of carbon atoms arranged in a honeycomb lattice structure, with strong carbon bonds and a bond distance of approximately 0.142 nm (Malard *et al*., 2009). Inorganic semiconductors such as Zinc oxide (ZnO) and titanium dioxide (TiO_2), Tungsten trioxide (WO_3), Zinc sulfide (ZnS), and Tin Oxide (SnO_2), which are metal oxides, have demonstrated

How to cite (APA):
Al-Shuwaili, M., Mahdi, H., & Makram M. (2024). Investigation of structural, morphology and optical properties of GO@metal oxide thin films prepared by spray pyrolysis technique. *New Materials, Compounds and Applications, 8*(2), 289-301 https://doi.org/10.62476/nmca82289

remarkable effectiveness in degrading organic pollutants and combating environmental pollution. (Selvakumar *et al*., 2023).

ZnO and TiO_2 have emerged as effective materials for photocatalytic wastewater treatment. ZnO is particularly notable for its cost-effectiveness, strong oxidation capacity, high photosensitivity, biocompatibility, satisfactory photocatalytic performance, chemical stability, and pyroelectric and piezoelectric properties. (Jamjoum *et al*., 2021). GO-based ZnO nanoparticles offer favorable physicochemical and photo-electrical properties, and the p-conjugation structure in GO enhances electronic mobility, improving ZnO photocatalysis. The exceptional specific surface area, active sites, and supportive properties of GO-based composites contribute to their efficiency in various photocatalytic applications (Haseen *et al*., 2020).

TiO_2 has demonstrated exceptional photocatalytic capabilities in various applications, including organic pollutant degradation and air purification. Graphene inclusion in TiO_2 composites enhances electron mobility, reduces recombination, prevents agglomeration, and increases active sites for pollutant degradation (Jamjoum *et al*., 2021; Tobaldi *et al*., 2021; Yaqoob *et al*., 2021). Similarly, the integration of metal and metal oxide nanoparticles, such as ZnO (Talib *et al*., 2022), TiO_2 (Azani *et al*., 2021), SiO_2 (Siwińska-Ciesielczyk et al., 2020), and Ag, with graphene has led to remarkable optoelectronic hybrid devices with enhanced responsivity for photodetector applications. Graphene's electrical and optical properties, combined with metal oxide nanostructures, unlock potential in photonics and optoelectronics, enabling applications like photodetectors, light-emitting devices, touch screens, transparent electrodes, and ultrahigh-frequency devices (Malard *et al*., 2009; Talib *et al*., 2022; Singh *et al*., 2011).

Azani et al. (2021), successfully synthesized a thin film of GO/TiO_2 using the sol-gel method and spin coating deposition technique with the aim of creating a self-cleaning coating. The introduction of GO induced significant changes in the microstructure, revealing the presence of the anatase phase of TiO_2. The resulting thin film exhibited super hydrophilic properties, demonstrated by a water contact angle of 4.11°. Moreover, the incorporation of GO led to a reduction in the band gap of TiO_2, promoting enhanced absorption and improved photodegradation performance. The GO/TiO_2 thin film achieved a methylene blue degradation rate of approximately 59% (Azani *et al*., 2021). Jalaukhan et al. (2021), conducted a study where thin films of SnO_2 and SnO_2/GO were fabricated using the spin coating method. Different concentrations of GO ranging from 0 to 4 g/ml were used in the fabrication process. X-ray diffraction (XRD) analysis confirmed the high crystallinity of the GO thin films. The band gap of pure SnO_2 was determined to be 3.56 eV, and interestingly, the band gap of the thin films increased with higher concentrations of GO, attributed to a reduction in particle size due to the increased GO concentration. Furthermore, the researchers evaluated the photocatalytic activity of the synthesized samples under UV light irradiation using Methyl Orange (MO) dye. The degradation efficiencies of SnO_2/GO-20 and SnO_2/GO-40 thin films were measured to be 2.2% and 3.4%, respectively. The prepared thin films demonstrated the ability to adsorb MO on both the surfaces of GO and metal oxides (Jalaukhan *et al*., 2021).

This study aimed to thoroughly examine the structural properties and morphology of nanocomposites containing graphene oxide and different metal oxides. Additionally, the objective was to conduct a comprehensive analysis to evaluate and compare the impact of the structural characteristics on the optical properties of these nanocomposites. The research focused on the crucial significance of graphene oxide and

its nanocomposites in order to gain valuable insights into their properties and potential applications.

2. Synthesis method

A modified Hummer method was utilized to synthesize graphene oxide colloid using graphite and potassium permanganate as precursors.

The first step in preparation of the GO@Ag solution was to ultrasonically treat the graphene oxide colloid for 30 minutes at a concentration of 1 mg/mL. Silver diamine hydroxide (40 M) was then prepared by combining ammonia, deionized water, and silver nitrate. In order to make the composite GO: Ag, $Ag(NH_3)OH$ and GO solutions at a ratio of 2:8 were mixed and stirred for 30 minutes, followed by half an hour in an oil bath at 70-80 °C. Lastly, the prepared solution was washed with deionized water three times before spraying.

As the next step of the synthesis procedure, the GO@Zn solution was prepared. Graphene oxide colloid was produced in a similar way to the previous step, GO@Ag solution preparation. After that, hexamethylene tetramine (0.2 M) and zinc acetate (0.2 M) were continuously added to the graphene oxide solution and stirred for 15 minutes. As a final step, the solution was placed in an oil bath for 3 hours at 90°C, washed three times with deionized water, and deposited.

The following step involves the preparation of Sol of GO@SiO_2. So, graphene oxide was mixed with ethanol at a concentration of 1 mg/ml and stirred. After adding 2 ml of TEOS to each of the above solutions, all mixtures were stirred together. A 24-hour waiting period was allowed for the final solution after diluting it with deionized water.

For the preparation of the tin oxide solution, 38 grams of tin chloride and 250 ml of ethanol were combined and stirred for 15 minutes, then settled overnight at room temperature. The SnO_2-GO composite solution was formed by adding graphene oxide up to 1 weight percent to the mixture of tin chloride and ethanol. A 15-minute stirring procedure followed by 30 minutes of ultrasonic treatment was carried out on the finished solution. In the next step, the final solution was kept for 24 hours. GO@SnO_2 was prepared by following these steps.

In order to prepare GO@TiO_2, the first step was to mix ethanol and acetic acid in a 1:10 ratio and stir for 15 minutes. After diluting the initial solution with titanium tetra isopropoxide drop by drop, it was kept at room temperature for 24 hours. After this, graphene oxide was applied to a concentration of up to 1%. Once that had been completed, the final solution was stirred for 15 minutes, followed by 30 minutes in the ultrasonic, and finally appeared for 24 hours.

The glass substrates were cleaned with an ultrasonic cleaner for 30 minutes to support the formation of the thin films. To create the thin films, 35 mL of each solution was sprayed using the spray pyrolysis method with compressed air as the carrier gas. The spray configurations include a nozzle spacing of 30-40 cm and a deposition rate of 2-2.5. For GO, GO@Ag, GO@Zn, GO@SiO_2, GO@SnO_2 and GO@TiO_2 thin films, the plate temperatures were set to 50, 150, 400, 400, 500 and 550 °C respectively.

3. Results and discussions

3.1. Structure description

X-ray diffraction crystallography of bare GO and GO containing Ag, Zn, SnO_2, TiO_2, and SiO_2 is shown in Figure 1. X-Ray Diffraction (XRD) is a powerful means for identifying the crystal structure of the atoms. It is based on the diffraction of X-ray beams by crystalline atoms into many specific directions. In order to determine the density of electrons in the crystal, we must measure the intensities and angles of the diffracted beams which will enable us to determine atom positions, chemical bonds, disorder, and other information related to the atoms (Waseda *et al*., 2011). According to Figure 1a, the bare graphene oxide exhibits a well-defined diffraction peak at 2θ ~ 11°. According to literature, the crystals are categorized into two groups, including true crystals (ordered long-range crystals) and amorphous crystals or pseudo crystals (short-range crystals). The latter commonly shows a sharp and narrow XRD peaks exhibiting the various phases available in the sample. On the other hand, the XRD peaks related to the pseudo crystals are typically broader. It is shown that the atoms of the GO are arranged in an AB stacking style, and their stacking height changes depending on the intensity of the oxidation. The peak located at 2θ ~ 11° corresponds to the (001), which is due to functional groups and the broad peak at 2θ ~ 24° may indicate the presence of graphite in the GO, which corresponds to the (002) plane (Sharma *et al.*, 2021).

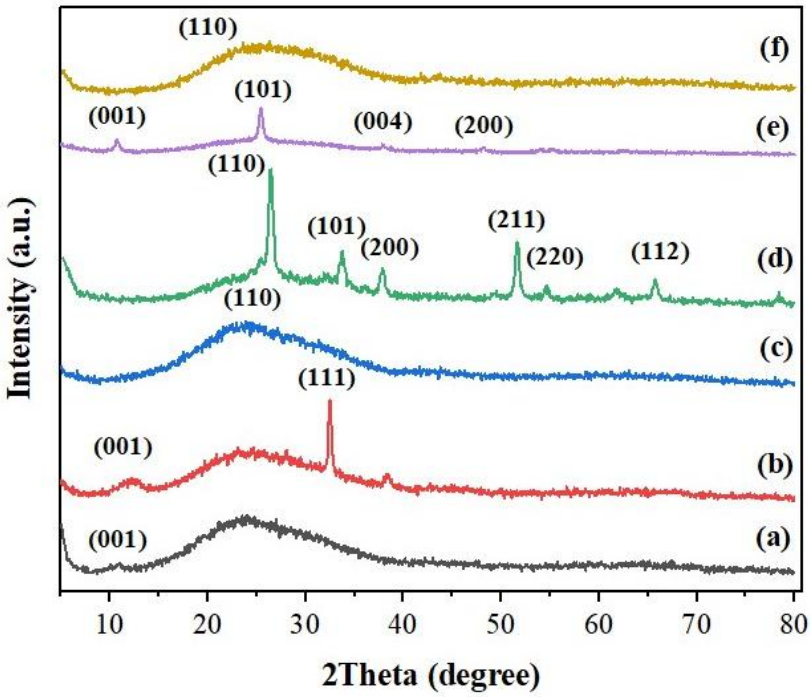

Figure 1. The XRD graphs of (a) bare GO, (b) GO@Ag, (c) GO@Zn, (d) GO@SnO_2, (e) GO@TiO_2, and (f) GO@SiO_2

XRD patterns of the GO-containing silver particles are shown in Figure 1b. A graphene oxide peak can also be observed in the GO@Ag nanocomposite. This peak is located at 2θ ~ 12.8°, which is imputed to the (001) basal plane. Interestingly, the XRD peak of GO shifted from 11° in the bare sample into 12.8° for the GO@Ag

nanocomposite. The Bragg's equation was adopted to calculate the interplanar spacing of GO d_{001} (Kahouli *et al*., 2015):

$$2d_{hkl}sin\theta = n\lambda. \quad (1)$$

In the above equation, d_{hkl} refers to the distance between the planes, h is the Bragg angle, n relates to the diffraction order and λ is the wavelength of the X-rays (λ = 1.541 Å). Accordingly, a d_{001} of 0.067 Å was obtained for the bare GO. However, the d_{001} of GO containing Ag nanoparticles is 0.087, indicating that the addition of silver nanoparticles to GO resulted in an increase in its basal plane interplanar spacing. Apart from the XRD peak of GO, a sharp and characteristic peak located at 2θ ~ 32.49° is found for the GO@Ag nanocomposite. Considering the face-centered cubic structure of Ag (fcc), the peak can be attributed to the crystallographic plane of (111) (Biswas *et al*., 2016; Noor *et al*., 2016; Lan *et al*., 2016). The peak clearly shows that the silver nanoparticles are present in the GO.

Debye-Scherrer equation can be used to determine the mean crystallite size of silver nanoparticles (Roncal-Herrero *et al*., 2011; Holzwarth & Gibson, 2011; Kalishwaralal *et al*., 2008):

$$D = \frac{K\,\lambda}{\beta\,cos\theta}\,. \quad (2)$$

Consequently, D is the mean particle size, K stands for the Scherrer constant (K = 0.98), λ denotes the wavelength of the X-ray (λ = 1.541 Å), and β indicates the full width at half maximum (FWHM).

Using the Equation 2, an average size of 4.05 Å is obtained for the GO@Ag nanocomposite. In Figure 1c, the XRD pattern of GO@Zn is illustrated. Unlike the GO@Ag sample, no peak related to the presence of the GO is observed for the sample containing the Zn nanoparticles. A broad peak can be found at 2θ ~ 24°, originating from the interaction between the Zn nanoparticles and GO, indicating that zinc is present within the nanocomposites (Taheri *et al*., 2019). By means of the Equation 2, an average crystallite size of 0.11 Å is attained for the GO@Zn sample.

According to the XRD pattern of the GO@SnO_2 nanocomposite (Figure 1d), the peaks at 2θ = 26.35, 33.7, 37.65, 51.6, 54.8, and 65.8 degrees are ascribed to the (110), (101), (200), (211), (220), and (112) crystallite facets of the SnO_2, attesting the existence of the SnO_2 in the body of the GO (Wang et al., 2013; Zheng et al., 2016). It has been calculated that the average size of the Sn nanoparticles is 3.05Å. The peak associated with the GO in GO@TiO_2 nanocomposites is found at 2θ ~ 10.76°. This peak is ascribed to the (001) basal plane and verifies the existence of the GO in the nanocomposite. Using the Equation 1, a d_{001} of 0.07 Å was calculated for this sample, which is higher than that obtained for the bare GO, implying that addition of TiO_2 nanoparticles increased the basal plane interplanar spacing of the graphene oxide. The (101), (004), and (200) crystal planes of anatase TiO_2 are related to the XRD peaks at 2θ = 25.4, 37.96, and 48.36 degrees, which lead to the production of the GO@TiO_2 nanocomposite (Liu *et al*., 2016). The average size of the TiO_2 particles was 1.06 Å.

According to Figure 1f, hybrid SiO_2-GO nanoparticles may be fully exfoliated in the composite containing SiO_2 nanoparticles, since the peak (2θ ~ 11°) corresponding to GO disappears in the SiO_2-containing sample. The broad peak at around 2θ ~ 25° is primarily because of the silica structure (Wu *et al*., 2015; Wang *et al*., 2022). An average size of 0.12 Å was calculated for the SiO_2 nanoparticles.

3.2. Morphology examination

Field emission scanning electron microscopy (FESEM) images of bare GO and GO with Ag, Zn, SnO_2, TiO_2, and SiO_2 are presented in Figure 2. In order to examine the morphology of materials, FESEM is a useful tool. This technique yields high resolution and detailed images of micro- to nano-structured materials by scanning their surfaces through focusing beam of electrons. Valuable information about the composition and topography of materials is provided by FESEM images (Crew *et al*., 1969). To investigate the chemical composition of the samples, energy-dispersive X-ray spectrometry (EDS) was also used.

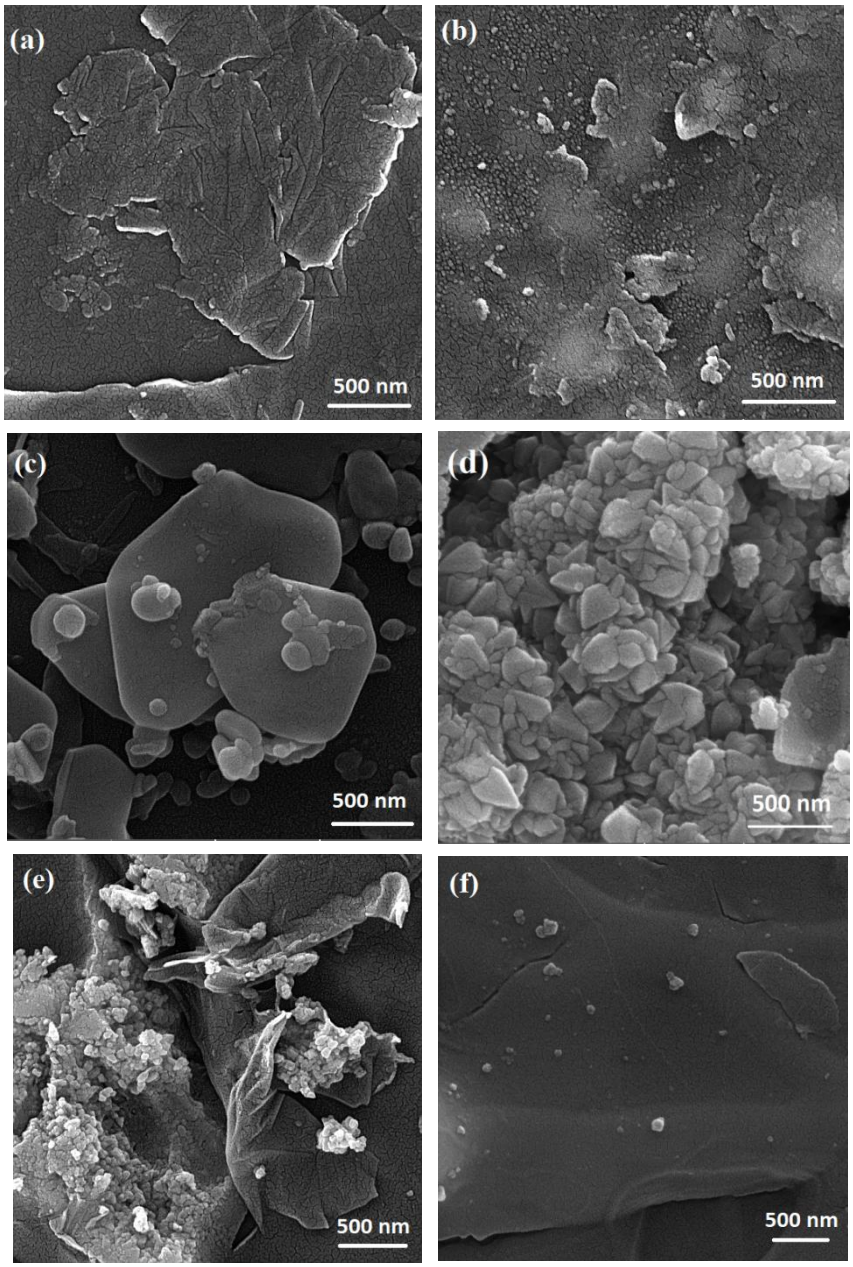

Figure 2. The FESM images of (a) bare GO, (b) GO@Ag, (c) GO@Zn, (d) GO@SnO_2, (e) GO@TiO_2, and (f) GO@SiO_2

FESEM image of the bare GO is given in Figure 2a. Clean and smooth sheets of graphene oxide are obviously observed.

Inclusion of silver nanoparticles into the graphene oxide changed the morphology of the GO and also its chemical composition, as evidenced by Figure 2b. Unlike the bare GO where the GO sheets can easily be observed, in the sample having silver nanoparticles, the GO sheets are cohered. Moreover, some spherical-like particles are found on the surface of GO, which can be attributed to the silver nanoparticles and subsequently corroborate the attachment of the Ag particles on the GO. In addition to FESEM, EDS pattern of the GO@Ag nanocomposite verifies the presence of the Ag particles on GO. In both EDS and FESEM patterns of the GO@Ag nanocomposite, Ag particles can be seen.

In Figure 2c, an image of GO obtained using FESEM anchoring with Zn is exhibited. Accordingly, the GO@Zn nanocomposite shows a crust-like morphology. In addition to crust-like particles, some spherical-like nanoparticles are found on the surface of the GO sheets, which are inclined to be distributed on GO. The spherical nanoparticles are attributed to ZnO particles with a size range of 10-40 nm.

The FESEM image of GO@SnO_2 nanocomposite is given in Figure 2d. A leaf-like structure is observed for the nanocomposite. Nanoparticles of SnO_2 have an average size of 200 nm. As can be seen in the FESEM image of the bare GO and the GO@SnO_2, the SnO_2 nanoparticles are anchored to the GO surface.

On the surface of the GO@TiO_2, as shown in Figure 2e, agglomerated spherical-like grains of TiO_2 can be found. The nanoparticles are about 50 nm in size and almost uniform in shape.

Figure 2f demonstrates the FESEM image of the GO@SiO_2 nanocomposite. Accordingly, the plain sheets of the GO are clearly observed. Comparing to the bare GO, the graphene sheets in GO@SiO_2 nanocomposite are smoother. Some nanoparticles are found on the surface of the GO, which can be imputed to the SiO_2 nanoparticles. Nanoparticles have an average size of about 50 nanometers.

3.3. Optical properties

3.3.1. The photoluminescence emission spectra

The photoluminescence (PL) emission spectra of bare GO and the GO@Ag, GO@Zn, GO@SnO_2, GO@TiO_2, and GO@SiO_2 nanocomposites are shown in Figure 3. PL spectroscopy is a powerful technique to examine the variation in different defects states available in materials. In addition, the analysis of photoluminescence spectra gives valuable information about the ability of immigration, charge carriers trapping, elimination of electron-holes and ultimately to study the recombination of electron-hole pairs in materials.

The PL principle involves the irradiation of light on the surface of the material, the excitation of electrons, the recombination of these photogenerated electrons with the holes, and ultimately the release of energy. There is a direct relationship between the intensity of the PL spectrum and the recombination of electron-hole pairs. There is less electron-hole pair recombination in PL spectra with low intensity, and more electron-hole pair recombination in PL spectra with high intensity. Consequently, the PL spectra with low intensity possess better photodegradation performance in photocatalytic activity (Rahman & Kar, 2020).

Referring to the PL spectrum of the GO (Figure 3a), a peak is observed at about 450 nm. The photoluminescence property of organic materials arises commonly from

four kinds of electronic transitions between the antibonding and the bonding molecular orbitals, including (1) $\sigma^* \rightarrow \sigma$ transition observed in alkanes, (2) $\sigma^* \rightarrow n$ transition occurs in alcohols, amines and ethers, (3) $\pi^* \rightarrow \pi$ transition takes place in alkenes, aldehydes, esters, and aromatic compounds, and (4) $\pi^* \rightarrow n$ transition occurs in ketones, aldehydes and esters. The first and fourth transitions have the largest and smallest energy gaps between their antibonding and bonding molecular orbitals, respectively. The peak at about 450 nm can therefore be attributed to the $\sigma^* \rightarrow n$ transition caused by hydroxyl groups on the surface of GO (Li *et al.*, 2012).

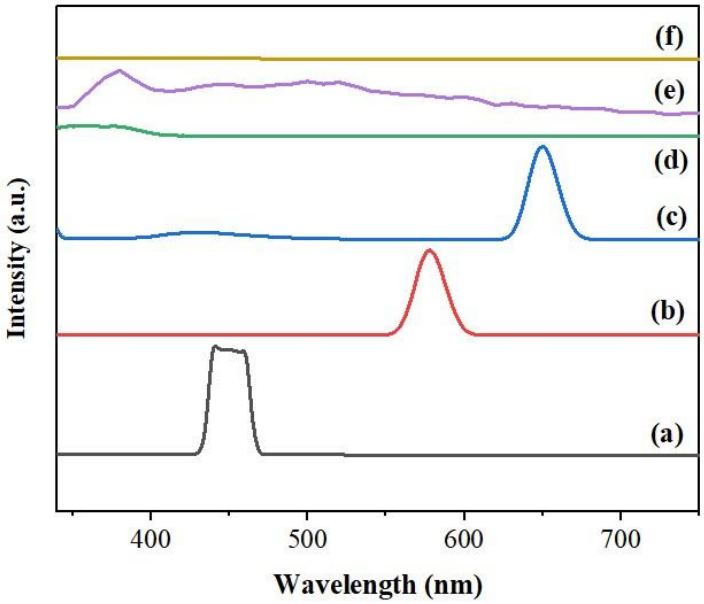

Figure 3. The PL emission spectra of (a) bare GO, (b) GO@Ag, (c) GO@Zn, (d) GO@SnO_2, (e) GO@TiO_2, and (f) GO@SiO_2

In Figure 3b, the PL spectrum of GO containing Ag nanoparticles is displayed at wavelengths ranging from 300 to 800 nm. An inclusion of Ag caused changes in the PL spectrum of the GO. The addition of Ag nanoparticles shifted the emission peak to a longer wavelength, showing a redshift and confirming the silver particles' attachment. Secondly, the introduction of Ag nanoparticles gave rise to a decrement in the intensity of PL emission peak. It has already been mentioned that a lower-intensity PL peak indicates less recombination of electron-hole pairs, which is positively affecting the photocatalytic activity of the nanocomposite. As a result, the inclusion of silver nanoparticles can enhance the performance of the nanocomposite. A peak located at 577 nm can be explained by the interaction between the luminescence of atomically layered GO and localized surface plasmon resonance of metallic silver nanoparticles (Lan *et al.*, 2014).

The PL emission spectrum of the GO@Zn nanocomposite is given in Figure 3c. Accordingly, a low-intensity peak is observed at about 350 nm, which is because of exciton recombination radiation. In addition to it, another sharp peak is found at approximately 650 nm. This peak is moved to a higher wavelength and is a redshift. The peak can originate from quantum confinement also high concentrations of point defects in the lattice. Compared to bare GO, the one containing zinc nanoparticles demonstrates less intensity, showing its better photocatalytic performance. Indeed, the better performance of GO@Ag nanocomposite can be due to the charge movement at the

interface and also the decrement in the hole-electron recombination, suggesting the photo-induced electrons originated in zinc are swiftly moved to GO. An additional route for the separation of charge carriers is provided by the GO layer, which functions as an electron sink (Al-Zahrani *et al*., 2023; Liu *et al*., 2013).

Figure 3d illustrates the PL emission spectrum of the GO@SnO_2, which obtained in the wavelength varying from 300 to 800 nm. Obviously, this nanocomposite shows no emission peak, and after 450 nm, the GO@SnO_2 has no emissions. Among all nanocomposites, the one containing SnO_2 nanoparticles showed the worst photocatalytic activity.

In Figure 3e of the PL emission spectrum, a broad peak is observed for GO@TiO_2 nanocomposite. This peak shows less intensity compared to the peak found in the GO, which is evidence for low hole-electron recombination and an excellent photocatalytic activity of the nanocomposite. In fact, in the nanocomposite, the Ti^{3+} ions serve as non-radiative trapping centers, preventing electron-hole recombination as well as enhancing photocatalysis.

As a result of the charge transfer between the GO and TiO_2 interfaces, the intensity of PL can be reduced. A reaction occurs between the electron-donating groups of GO and the electron-withdrawing groups of O=T=O in TiO_2 in GO@TiO_2 nanocomposite. As a result of this reaction, electron mobility increases in the nanocomposite, and single excitons are also generated. By leaving electrons in TiO_2 nanoparticles and holes in GO, excitons are separated from the GO-metal oxide interface (Phanichphant *et al*., 2019; Singh *et al*., 2021; Rahman & Kar, 2020).

The PL emission spectrum of GO@SiO_2 nanocomposite is shown in Figure 3f. Accordingly, no emission is recorded. Moreover, no PL emission peak is observed for the nanocomposite. Like the sample with SnO_2, the GO@SiO_2 nanocomposite cannot be a good choice for optical activity.

3.3.2. UV-Visible absorption spectra

In Figure 4, UV-Visible spectra for bare GO and nanocomposites of GO@Ag, GO@Zn, GO@SnO_2, GO@TiO_2, and GO@SiO_2 are displayed. Analyzing UV/VIS wavelengths absorbed or transmitted by a sample can be performed using UV-Visible spectroscopy, an advantageous analytical tool.

A weak absorption peak at about 355 nm can be detected in Figure 4a, based on the UV-Visible spectrum of the bare GO. The peak is ascribed to the $\pi^* \rightarrow n$ electronic transition observed on the surface of GO caused by various oxygen-containing functional groups, including COOH, CHO, and C–O–C (Najafi *et al*., 2017; Hareesh *et al.,* 2016). Due to the presence of hydroxyl groups on the surface of GO, a peak was also found at approximately 450 nm, which correlated with the electronic transition in PL spectroscopy. It can be concluded that GO was synthesized based on the peaks mentioned above.

Figure 4b illustrates the UV-Visible spectrum of the GO containing the Ag nanoparticles. An absorption peak is observed at about 350 nm. Worth mentioning that introduction of Ag nanoparticles into the GO shifted a little the absorption peak of GO from 355 to 350 nm, which a blueshift occurs. The peak located at 355 nm corresponds to surface plasmon resonance of Ag nanoparticles (Hareesh *et al.,* 2016). There is good agreement between this peak and the PL emission peak at 577 nm. The PL emission spectrum was therefore explained by the interaction between the luminescence of

atomically layered GO and localized surface plasmon resonance of metallic silver nanoparticles.

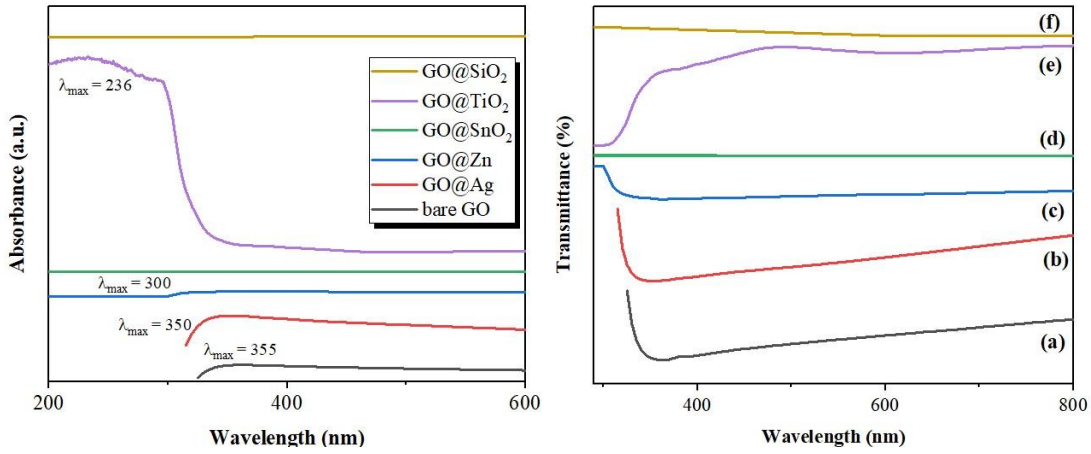

Figure 4. The UV-Visible and transmittance spectra of (a) bare GO, (b) GO@Ag, (c) GO@Zn, (d) $GO@SnO_2$, (e) $GO@TiO_2$, and (f) $GO@SiO_2$

A UV-Visible spectrum of the GO@Zn nanocomposite can be found in Figure 4c. The GO@Zn nanocomposite shows a weak peak at about 300 nm, meaning that inclusion of zinc nanoparticles shifted the absorption peak of GO to the lower wavelength. This peak matches the PL emission peak at 650 nm, which was explained by the existence of defects in the structure of the nanocomposite. Referring to the UV-Visible spectrum of the $GO@SnO_2$, no absorption peak seen for this nanocomposite, which is in consistent with the PL results. Accordingly, no peak was observed in the emission spectrum of the $GO@SnO_2$.

For the nanocomposite containing TiO_2 nanoparticles, an absorption peak found at approximately 236 nm, which is a blue-shifted. The movement of the wavelength to lower amounts can be explained by partially restoring the π-conjugation network of the nanocomposite after exposure to heating. A pathway for electron transfer can be provided by the reaction between the functional groups on the GO and the Ti ions (Najafi *et al*., 2017). Like the $GO@SnO_2$ sample, the one having SiO_2 nanoparticles exhibits no absorption peak, which is in agreement with the PL results where no PL emission peak was found for this nanocomposite.

The following equation can be used to calculate the band gap energy (E_g) of the samples (Lee *et al*., 2021).:

$$E_g = h \times \vartheta = \frac{h \times c}{\lambda_g} . \quad (3)$$

Considering c is the speed of light (3×10^8 m s^{-1}), λ represents the wavelength, and h is the Planck constant (6.626×10^{-34} J s).

According to Equation 3, there is a reverse relationship between the band gap energy and the wavelength, meaning that less wavelength, more band gap energy. The λ_g of the bare GO, GO@Ag, GO@Zn, $GO@SnO_2$, $GO@TiO_2$, and $GO@SiO_2$ were respectively 355, 350, 300, 0, 236, and 0 nm. Among the samples, the one including TiO_2 nanoparticles demonstrates the least wavenumber and subsequently the highest band gap energy. The point here is that negligible difference observed among the

wavelength of the samples; therefore, the band gap energies of the nanocomposites doesn't vary significantly.

4. Conclusion

In this study, the optical behavior of the GO and its nanocomposites, including GO@Ag, GO@Zn, GO@SnO_2, GO@TiO_2, and GO@SiO_2 was investigated. As the characterization tests of XRD, and FESEM, corroborated, the nanocomposites were successfully synthesized. In terms of XRD test, the planes of (001) and (111) observed for the GO@Ag corroborate the synthesis of this nanocomposite. The attachment of zinc nanoparticles to the surface of GO was demonstrated by (110). The planes of (110), (101), (200), (211), (220) and (112) verify that the SnO_2 nanoparticles are available in the structure of the GO@ SnO_2. Moreover, the (001), (101), (004), (200), and (110) crystallite planes testify the synthesis of the GO@TiO_2. In addition, the broad peak located at the plane of (110) was evidence for the successfully fabrication of GO@SiO_2. FESEM images exhibited that the morphology of the nanocomposites is completely different, which is another evidence for the synthesis of the nanocomposites.

Among the samples, the one containing TiO_2 nanoparticles showed the best performance in PL and UV analyses. The reason behind the high photocatalytic activity of GO@TiO_2 nanocomposite is that the titanium ions act as trappings centers, which are beneficial for inhibition of electron-hole pairs recombination. Another reason is that the electron-withdrawing group of (O=T=O) in TiO_2 reacts with the electron-donating functional groups on GO, which provides pathways for electrons transfer and accelerates their mobility.

References

Al-Zahrani, S.A., Umar, K., Tweib, S.A., Rashd, J.A.M., Afridi, S.K., Bhawani, S.A., ... & Ayyar, M. (2023). Biomass mediated synthesis of ZnO and ZnO/GO for the decolorization of methylene blue under visible light source. *Catalysts*, *13*(2), 409.

Azani, A., Halin, D.S.C., Abdullah, M.M.A.B., Razak, K.A., Razak, M.F.S.A., din Ramli, M.M., ... & Chobpattana, V. (2021). The effect of go/tio_2 thin film during photodegradation of methylene blue dye. *Evergreen*, *8*(3), 556-564.

Biswas, S., Kole, A.K., Tiwary, C.S., & Kumbhakar, P. (2016). Enhanced nonlinear optical properties of graphene oxide–silver nanocomposites measured by Z-scan technique. *RSC Advances*, *6*(13), 10319-10325.

Chen, D., Xin, Y., Lu, B., Pan, X., Huang, J., He, H., & Ye, Z. (2020). Self-powered ultraviolet photovoltaic photodetector based on graphene/ZnO heterostructure. *Applied Surface Science*, 529, 147087.

Crewe, A.V., Isaacson, M., & Johnson, D. (1969). A simple scanning electron microscope. *Review of Scientific Instruments*, *40*(2), 241-246.

Das, A., Mondal, S.R., & Palai, G. (2020). Realization of graphene based quantum dot solar cell through the principle of photonics. *Optik*, 221, 165283.

Gao, F., Liu, K., Cheng, R., & Zhang, Y. (2020). Efficiency enhancement of perovskite solar cells based on graphene-CuInS2 quantum dots composite: The roles for fast electron injection and light harvests. *Applied Surface Science*, 528, 146560.

Hareesh, K., Williams, J. F., Dhole, N. A., Kodam, K. M., Bhoraskar, V. N., & Dhole, S. D. (2016). Bio-green synthesis of Ag–GO, Au–GO and Ag–Au–GO nanocomposites using Azadirachta indica: its application in SERS and cell viability. *Materials Research Express*, *3*(7), 075010.

Haseen, U., Umar, K., Ahmad, H., Parveen, T., & Mohamad Ibrahim, M. N. (2020). Graphene and its composites: applications in environmental remediation. *Modern Age Waste Water Problems: Solutions Using Applied Nanotechnology*, 85-91.

Holzwarth, U., Gibson, N. (2011). The Scherrer equation versus the'Debye-Scherrer equation'. *Nature Nanotechnology*, *6*(9), 534-534.

Jalaukhan, A.H.A., Shohany, B.G., & Etefagh, R. (2021). Preparation and investigation of optical properties and photocatalytic activity of SnO2/GO thin films. *Scientia Iranica*, 28, 1908-1916.

Jamjoum, H.A.A., Umar, K., Adnan, R., Razali, M.R., & Mohamad Ibrahim, M.N. (2021). Synthesis, characterization, and photocatalytic activities of graphene oxide/metal oxides nanocomposites: *A review*. *Frontiers in Chemistry*, 9, 752276.

Kahouli, M., Barhoumi, A., Bouzid, A., Al-Hajry, A., & Guermazi, S. (2015). Structural and optical properties of ZnO nanoparticles prepared by direct precipitation method. *Superlattices and Microstructures*, 85, 7-23.

Kalishwaralal, K., Deepak, V., Ramkumarpandian, S., Nellaiah, H., & Sangiliyandi, G. (2008). Extracellular biosynthesis of silver nanoparticles by the culture supernatant of Bacillus licheniformis. *Materials Letters*, *62*(29), 4411-4413.

Kumar, N., Srivastava, V.C. (2018). Simple synthesis of large graphene oxide sheets via electrochemical method coupled with oxidation process. *ACS omega*, *3*(8), 10233-10242.

Lan, N.T., Dinh, N.X., Hung, N.D., Lan, H., Tuan, P.A., Trung, N.N., ... & Le, A.T. (2014). Photochemical decoration of silver nanoparticles on graphene oxide nanosheets and their optical characterization. *Journal of Alloys and Compounds*, 615, 843-848.

Lan, N.T., Dinh, N.X., Hung, N.D., Lan, H., Tuan, P.A., Trung, N.N., ... & Le, A.T. (2014). Photochemical decoration of silver nanoparticles on graphene oxide nanosheets and their optical characterization. *Journal of Alloys and Compounds*, 615, 843-848.

Lee, A.Y., Yang, K., Anh, N.D., Park, C., Lee, S.M., Lee, T.G., & Jeong, M.S. (2021). Raman study of D* band in graphene oxide and its correlation with reduction. *Applied Surface Science*, 536, 147990.

Li, M., Cushing, S. K., Zhou, X., Guo, S., & Wu, N. (2012). Fingerprinting photoluminescence of functional groups in graphene oxide. *Journal of Materials Chemistry*, *22*(44), 23374-23379.

Liu, J., Niu, Y., He, X., Qi, J., & Li, X. (2016). Photocatalytic Reduction of CO2 Using TiO2- Graphene Nanocomposites. *Journal of Nanomaterials*, *2016*(1), 6012896.

Liu, Y.Z., Li, Y.F., Yang, Y.G., Wen, Y.F., & Wang, M.Z. (2013). A one-pot method for producing ZnO–graphene nanocomposites from graphene oxide for supercapacitors. *Scripta Materialia*, *68*(5), 301-304.

Malard, L.M., Pimenta, M.A., Dresselhaus, G., & Dresselhaus, M.S. (2009). Raman spectroscopy in graphene. *Physics Reports*, *473*(5-6), 51-87.

Moon, S.H., Jeong, J., Kim, G.W., Jin, D.K., Kim, Y.J., Kim, J.K., ... & Hong, Y.J. (2020). Van der Waals gap-inserted light-emitting p–n heterojunction of ZnO nanorods/graphene/p-GaN film. *Current Applied Physics*, *20*(2), 352-357.

Najafi, M., Kermanpur, A., Rahimipour, M.R., & Najafizadeh, A. (2017). Effect of TiO2 morphology on structure of TiO2-graphene oxide nanocomposite synthesized via a one-step hydrothermal method. *Journal of Alloys and Compounds*, 722, 272-277.

Noor, A.A.M., Rameshkumar, P., Huang, N.M., & Wei, L.S. (2016). Visual and spectrophotometric determination of mercury (II) using silver nanoparticles modified with graphene oxide. *Microchimica Acta*, 183, 597-603.

Phanichphant, S., Nakaruk, A., Chansaenpak, K., & Channei, D. (2019). Evaluating the photocatalytic efficiency of the BiVO4/rGO photocatalyst. *Scientific Reports*, *9*(1), 16091.

Rahman, K. H., & Kar, A. K. (2020). Titanium-di-oxide (TiO2) concentration-dependent optical and morphological properties of PAni-TiO2 nanocomposite. *Materials Science in Semiconductor Processing*, 105, 104745.

Roncal-Herrero, T., Rodríguez-Blanco, J.D., Oelkers, E.H., & Benning, L.G. (2011). The direct precipitation of rhabdophane (REEPO4• n H2O) nano-rods from acidic aqueous solutions at 5–100° C. *Journal of Nanoparticle Research, 13*(9), 4049-4062.

Rong, X., Qiu, F., Zhang, C., Fu, L., Wang, Y., & Yang, D. (2015). Preparation, characterization and photocatalytic application of TiO2–graphene photocatalyst under visible light irradiation. *Ceramics International, 41*(2), 2502-2511.

Selvakumar, K., Oh, T. H., Arunpandian, M., Aruchamy, K., & Polisetti, V. (2023). Hydrothermal Fabrication of GO Decorated Dy2WO6-ZnO Ternary Nanocomposites: An Efficient Photocatalyst for the Degradation of Organic Dye. *Applied Sciences, 13*(12), 7145.

Sharma, N., Tomar, S., Shkir, M., Choubey, R.K., & Singh, A. (2021). Study of optical and electrical properties of graphene oxide. *Materials Today: Proceedings*, 36, 730-735.

Shimomura, K., Imai, K., Nakagawa, K., Kawai, A., Hashimoto, K., Ideguchi, T., & Maki, H. (2021). Graphene photodetectors with asymmetric device structures on silicon chips. *Carbon Trends*, 5, 100100.

Singh, B. P., Huang, C. Y., Singh, D. P., Palani, P., Duponchel, B., Sah, M., ... & Pandey, K. K. (2021). The scientific duo of TiO2 nanoparticles and nematic liquid crystal E204: Increased absorbance, photoluminescence quenching and improving response time for electro-optical devices. *Journal of Molecular Liquids*, 325, 115130.

Singh, V., Joung, D., Zhai, L., Das, S., Khondaker, S.I., & Seal, S. (2011). Graphene based materials: past, present and future. *Progress in Materials Science, 56*(8), 1178-1271.

Siwińska-Ciesielczyk, K., Świgoń, D., Rychtowski, P., Moszyński, D., Zgoła-Grześkowiak, A., & Jesionowski, T. (2020). The performance of multicomponent oxide systems based on TiO2, ZrO2 and SiO2 in the photocatalytic degradation of Rhodamine B: mechanism and kinetic studies. *Colloids and Surfaces A: Physicochemical and Engineering Aspects*, 586, 124272.

Taheri, N.N., Ramezanzadeh, B., & Mahdavian, M. (2019). Application of layer-by-layer assembled graphene oxide nanosheets/polyaniline/zinc cations for construction of an effective epoxy coating anti-corrosion system. *Journal of Alloys and Compounds*, 800, 532-549.

Tobaldi, D.M., Dvoranová, D., Lajaunie, L., Rozman, N., Figueiredo, B., Seabra, M.P., ... & Labrincha, J.A. (2021). Graphene-TiO2 hybrids for photocatalytic aided removal of VOCs and nitrogen oxides from outdoor environment. *Chemical Engineering Journal*, 405, 126651.

Wang, B., Guan, D., Gao, Z., Wang, J., Li, Z., Yang, W., & Liu, L. (2013). Preparation of graphene nanosheets/SnO2 composites by pre-reduction followed by in-situ reduction and their electrochemical performances. *Materials Chemistry and Physics, 141*(1), 1-8.

Wang, Y., Wu, M., Lu, P., Wang, C., Shi, X., Ye, X., & Miao, X. (2022). Effect of 1wt% GO, MWCNTs, SiO2-GO and SiO2-MWCNTs on mechanical properties and corrosion resistance of double-layer zinc silicate coatings. *Journal of Inorganic and Organometallic Polymers and Materials, 32*(11), 4384-4400.

Waseda, Y., Matsubara, E., & Shinoda, K. (2011). *X-ray diffraction crystallography: introduction, examples and solved problems*. Springer Science & Business Media.

Wu, G., Ma, L., Liu, L., Chen, L., & Huang, Y. (2015). Preparation of SiO2–GO hybrid nanoparticles and the thermal properties of methylphenylsilicone resins/SiO2–GO nanocomposites. *Thermochimica Acta*, 613, 77-86.

Yaqoob, A. A., Ibrahim, M. N. M., Ahmad, A., & Vijaya Bhaskar Reddy, A. (2021). Toxicology and environmental application of carbon nanocomposite. *Environmental remediation through carbon based nano composites*, 1-18.

Zheng, W., Li, S., Yu, X., Chen, C., Huang, H., Huang, Y., & Li, L. (2016). Synthesis of hierarchical reduced graphene oxide/SnO2/polypyrrole ternary composites with high electrochemical performance. *Materials Research Bulletin*, 80, 303-308.